Low-energy electron diffraction study of oxygen-induced reconstructions on Cu(210)

Y. P. Guo, K. C. Tan, H. Q. Wang, C. H. A. Huan, and A. T. S. Wee*
Department of Physics, National University of Singapore, 2 Science Drive 3, Singapore 117542
(Received 3 April 2001; revised manuscript received 8 February 2002; published 17 October 2002)

The oxygen-induced reconstructions on Cu(210) have been investigated by low-energy electron diffraction (LEED). The adsorption of oxygen on Cu(210) leads to a series of $(n\times1)$ $(n=2,3)$ reconstructions comprising Cu-O chains along the [001] direction on the topmost layer. The Cu(210)-(2×1)O structure is found to be the most thermodynamically favorable phase. A quantitative LEED analysis, performed by comparing the simulation results of different 2×1 and 3×1 models, confirms an added row model with oxygen sitting on the long bridge sites along the [001] direction. The oxygen atoms sit in a deeper position from the surface than the topmost Cu atoms, and the Cu-O rows relax upward. In the Cu(210)-(3×1)O structure with an oxygen coverage of $\frac{2}{3}$ ML, oxygen atoms reside deeper than the accompanying Cu atoms in one Cu-O row, while in the adjacent row, oxygen sits higher than the Cu atoms. The nearest and second nearest neighbor Cu-O distances are determined to be 1.82 ± 0.03 and 1.96 ± 0.06 Å respectively for both 2×1 and 3×1 reconstructions. The formation of relatively strong Cu-O bonds appears to be the driving force for both reconstructions.

DOI: 10.1103/PhysRevB.66.165410 PACS number(s): 68.35.Bs, 61.14.Hg

INTRODUCTION

Oxygen-induced reconstructions and self-organization behavior on transition-metal fcc(110) surfaces have been subjects of recent fundamental interest.[1–6] The topmost atom layer on such surfaces generally shows a strong tendency to reconstruct upon oxygen adsorption, and could serve as the template for growth of one- or two-dimensional periodic nanostructures. It has been well established that what forms on Cu(110), Ag(110), and Ni(110) surfaces is a so-called added-row structure in the form of metal-oxygen chains aligned along the [001] direction.[7–12] Scanning tunneling microscopy (STM) studies revealed that the dissociative adsorption of oxygen induces three reconstructions on Ni(110) identified as 3×1, 2×1, and 3×1 structures in this sequence with increasing oxygen coverage.[11] Total-energy calculations show that the interaction between the oxygen *p* states and the metal *d* states can give rise to a bonding downshift of the *p* states and to antibonding states that are partly shifted above the *d* bands. The antibonding states are less occupied for oxygen on the reconstructed Cu(110) surface than on the unreconstructed one.[13] Oxygen atoms are strongly bound to the low-coordinated metal atoms to compensate for the energetic cost of breaking metal-metal bonds.[7,14] The growth of oxygen-induced structures on the underlying metal surfaces depends on the attractive metal-oxygen and the repulsive O-O interactions, the bond strength and cohesive energy of metal atoms, as well as the atom-atom separation along [110] and [001] directions. It would be interesting to see if the formation of the Cu-O chains is an intrinsic behavior of oxygen chemisorption on Cu(n10) surfaces $(n=1,2,3,4,...)$ in general, and if adsorbed oxygen on higher-index Cu planes occupies similar sites as those on low-index surfaces. Surface-extended x-ray-absorption fine-structure (SEXAFS) studies showed that on the Cu(210) surface, oxygen adsorption induces a missing row reconstruction with the missing row along [001] direction.[7] STM observations of the interaction of oxygen on Cu(210) gave a direct measurement of the larger inter-row spacing of 8.08 Å in the Cu(210)-(2×1)O structure.[15] Isolated Cu-O rows nucleate and lengthen through trapping of mobile Cu and O atoms at ends of the chains supporting the added row model. Knight, Driver, and Woodruff[16,17] found, by STM, that there exists one common structural model for Cu($4n$ 1 0) surfaces $(n=1,2,3,...)$, three adjacent [001] Cu atom rows and one missing row comprising the Cu(100) $(\sqrt{2}\times2\sqrt{2})R45°$-O surface, and it was suggested that more such surfaces need to be studied, especially by quantitative structural methods such as low-energy electron diffraction (LEED).[18]

In this paper, we determine the O-induced reconstructions on Cu(210) between 300–700 K by tensor LEED analysis. This study also investigates how the formation of O-induced reconstructions on the topmost Cu layer affects the relaxations of the second and third sublayers.

EXPERIMENT

The LEED experiments were carried out *in situ* in a μ-metal shielded ultra high-vacuum (UHV) chamber equipped with rear-view LEED optics. The base pressure of this UHV system was less than 7×10^{-10} mbar. A polished Cu(210) single crystal with a diameter of 12 mm and a thickness of 2 mm was mounted on a precision manipulator, which allowed optimum alignment for normal incidence of the electron beam, and appropriate thermal treatment. Before LEED measurements, the Cu(210) crystal was cleaned by repeated cycles of Ar^+ bombardment for 30 min (1.5 keV, 18 μA) followed by subsequent annealing (900 K, 30 min). Sample cleanliness was checked by Auger electron spectroscopy, as well as the comparison of sharpness and intensity of the individual 1×1 LEED spots from different runs of measurements. LEED intensities of 13 diffracted beams were recorded at normal incidence by an analog/digital data acquisition system, out of which five beams fall into the (001) surface mirror plane, giving a total of eight symmetrically inequivalent beams. The energy range of the spectra was 28–300 eV. While the intensity of some beams can only be detected in a shorter energy range than 28–300 eV, the cu-

mulative energy range of the eight symmetrically inequivalent beams for clean Cu(210) is determined to be 1360 eV. The background subtraction for each spot was performed by the procedure described in Ref. 19. Furthermore, the intensity was normalized to the current of the incident electron beam at the corresponding energy. Several sets of independent data were measured and compared, ensuring very small deviations between the experimental curves.

For oxygen uptake experiments, oxygen gas was introduced into the UHV chamber via a precision leak valve, and the pressure measured by an uncalibrated ion gauge. In order to qualitatively determine the structural rearrangement induced by oxygen chemisorption, dynamical observations of LEED patterns were conducted while exposing the bare Cu(210) surface to oxygen partial pressures of 5×10^{-9} mbar at 300, 450, 550, and 700 K, respectively. In addition, to effectively control the O exposure on Cu(210) for careful *IV*-LEED measurements, static O uptake experiments were also performed.

The surface structural analysis was carried out by the tensor LEED approach using the symmetrized automatic tensor LEED program (SATLEED) provided by Van Hove *et al.*[20] Considering the fact that the renormalized forward scattering (RFS) does not converge well due to divergences in the underlying LEED theory for atomic plane spacings of less than 1 Å, as well as Pendry's empirical approximation that the effective number of calculated planes should be about 8 for clean Cu(210),[21] we organized thick ''composite layers'' with ten ''simple layers'' (each containing one atom for two-dimensional 1×1 periodicity) combined in one single ''composite layer'' to avoid convergence problems in RFS perturbation. Below this composite overlayer, another double-layer stacking was organized for the doubling. The decay component of the forward plane wave was carefully monitored in the approach, by properly setting the corresponding parameter (the parameter which limits the decay of plane waves from one layer to the next layer was set to <0.001), ensuring that the forward component decays to a negligible value inside the thick composite layers. The backscattering contribution from the deeper layers constructed by the interlayer bulk vector in the program therefore became less pronounced in the LEED search. Accordingly, for the added row 2×1 reconstruction on Cu(210), we assembled the first ''composite layer'' composed of one 2×1 O sublayer, one 2×1 Cu sublayer and eighteen 1×1 Cu sublayers. For the 3×1 reconstruction with an oxygen coverage of 0.66, two 3×1 O sublayers, two 3×1 Cu sublayers, and 15 1×1 Cu sublayers were included in one single ''composite layer'' on the surface. Using such composite layers in RFS had given good convergent results.

During the first three tensor LEED cycles, the coordinates of all atoms in the first composite layer were allowed to change. Subsequently, only those in the first ten sublayers were optimized while the others were fixed. All the integer and fractional beams were assigned the same weighting factor, and the agreements between experimental and theoretical data were compared using the reliability factor R_P. Eight phase shifts were calculated using the phase shift package by Barbieri and Van Hove.[20] The imaginary part of the inner potential was optimized and then fixed at -4.0 eV and the real part of the inner potential was refined as one parameter during the tensor LEED search. The Debye temperatures used in the calculations were 427 K for O, 315 K for 1×1 Cu, and 300 K for 2×1 and 3×1 Cu respectively.

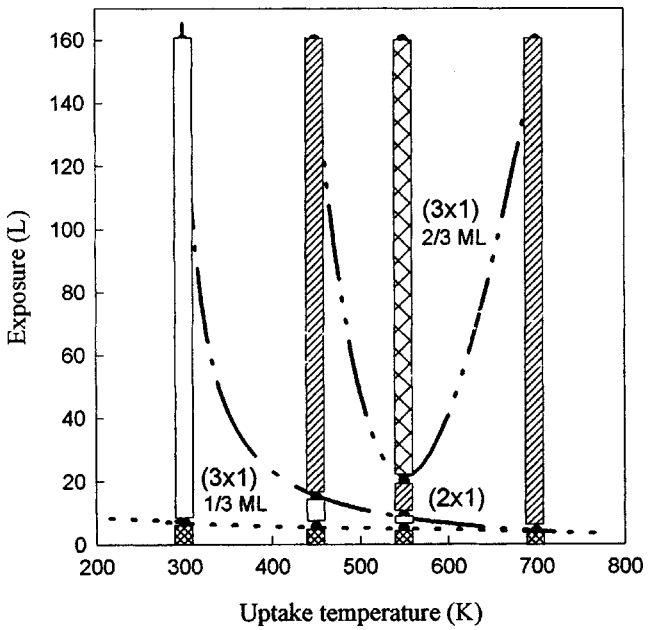

FIG. 1. The O-induced reconstructions on Cu(210) determined by LEED as a function of O exposure and uptake temperature. The bars represent experimental data recorded dynamically during oxygen uptake. The dashed lines define the separation of different ($n \times 1$) phases.

RESULTS AND DISCUSSION

Figure 1 summarizes the dynamic LEED observations of oxygen-induced reconstructions for oxygen exposures ranging from 0.01 to 160 L at substrate temperatures of 300, 450, 550, and 700 K, respectively. This phase diagram was obtained by measuring the positions and intensities of all the possible diffracted beams simultaneously as a function of oxygen exposure and uptake temperature. As shown in Fig. 1, 3×1 and 2×1 reconstructions are formed on the Cu(210) surface depending on temperature and oxygen exposure. At relatively low oxygen exposures (<5 L), the LEED pattern did not show clear periodicity with the appearance of weak streaks between 1×1 integer beams in the temperature range of 300–700 K. We attribute this to a transition phase prior to the formation of 3×1 and 2×1 reconstructions. In the transition phase O atoms tend to avoid sharing Cu atoms, so that each O adatom creates areas where the adsorption of additional adatoms is unfavorable.[22] The growth of Cu-O chains to form the 3×1 and 2×1 phases is limited by the number of available O adatoms.

With increasing oxygen dosage on Cu(210) at 300–550 K, the 3×1 pattern gradually strengthens and becomes sharpest at 8 L. The 3×1 phase remains unchanged for oxygen exposures up to 160 L at room temperature. At uptake temperatures >300 K, the 3×1 phase undergoes a transfor-

mation to a 2×1 phase with increasing oxygen coverage. Furthermore at 550 K, another 3×1 phase forms at higher oxygen coverage than the 2×1 reconstruction. Although the two 3×1 phases show similar LEED patterns, they are not attributed to the same structures. We postulate the higher coverage 3×1 phase at 550 K to be the O-induced reconstruction with $\frac{2}{3}$-ML oxygen coverage, which we confirm by *IV*-LEED calculations. No 1×1 LEED pattern attributed to full coverage was also observed at higher oxygen exposures up to 250 L on Cu(210). Gruzalski *et al.*[23] found that it was difficult to increase the coverage beyond 0.66 ML for oxygen adsorption on Cu(110). This suggests that there is significant repulsive interaction between the tightly paired Cu-O chains and/or O adatoms, maximizing the separation at high oxygen coverage. Figure 1 also shows that, at 700 K, the oxygen uptake rate is reduced due to the competing process of oxygen desorption. The formation of the 2×1 reconstruction is achieved either by direct exposure at elevated temperatures or by thermal treatment of other structures such as the 3×1 phase with $\frac{2}{3}$-ML oxygen coverage.

On the basis of the present LEED observations that the low-coverage 3×1 phase transforms to the 2×1 structure and finally the higher coverage 3×1 structure, we postulate that the formation mechanism involves diffusion of Cu-O chains with oxygen adsorption at the long bridge sites, as described by the ''added row'' model.[2,10,24] According to first-principles calculations of oxygen adsorption on Cu(110) surface (where the formation energy of an isolated Cu-O pair in the [001] direction is -0.53 eV),[22] individual Cu adatoms from the terrace edges are sufficiently mobile at room temperature and are easily trapped on the flat terrace by coadsorbed oxygen atoms due to the high activity of O adatoms. The Cu and O adatom pairs are eventually stabilized and become nuclei for the formation of new rows. When additional Cu and O adatoms are attached to the nucleus, the growth of Cu-O-Cu chains occurs. During the growth of the chains, the configuration of the chains maintains the largest separation between O adatoms due to interchain repulsion and the strong bonding between Cu and O adatoms along the [001] direction. With increasing length, the resulting Cu-O chains become stabilized and lose mobility. When two or more such chains propagate together in islands, depending on the oxygen coverage, the structure with a local 3×1 or 2×1 periodicity is distinguished by LEED. Based on first principles calculation and diffusion mechanisms of Cu and O adatoms,[22] the growth of the chains occurs close to terrace edges and the chain length is limited by the number of Cu atoms evaporating from terrace steps. The preferred growth of the chains along the [001] direction is related to the higher diffusion barriers in this direction, compared with the corresponding value along the $[1\bar{2}0]$ direction. As argued by Coulman *et al.*,[2] the attraction between the chains and adatoms is the strongest in the [001] direction, leading to a preferential growth of $n\times1$ nuclei.

Tensor LEED calculations were next performed to determine the detailed geometrical parameters that could give the best match to the experimental intensity curves. The selected structures for the Cu(210) (2×1)-O ($\frac{1}{2}$-ML coverage) and (3×1)-O ($\frac{2}{3}$-ML coverage) surfaces correspond to oxygen exposures of 9 and 24 L at 550 K, respectively. In detail, for the O-induced 2×1 reconstruction with an oxygen exposure of 9 L at 550 K, we have done tensor LEED calculations of over 30 trial structures. To simplify, here we present four models for the Cu(210)-(2×1)O reconstruction; they are models $M1$, $M2$, and $M3$ for the added row structures and the buckled row (BR) model, as illustrated in Fig. 2. In model $M1$, the oxygen atoms occupy the long bridge sites between two Cu atoms while Cu-O rows reside on the topmost Cu layer maintaining Cu fcc symmetry. In model $M2$, the oxygen atoms still occupy the long bridge site with Cu-O rows on hcp sites relative to the second Cu layer. Model $M3$ has oxygen atoms at the fourfold hollow site and the Cu-O rows are sited according to the fcc structure as in model $M1$. After tensor LEED calculations, the optimized R_p values are 0.237, 0.419, and 0.434 for $M1$, $M2$, and $M3$ models respectively. Clearly the R_p values for the models $M2$ and $M3$ are too high to be acceptable models for the (2×1)-O structure. The BR model was also analyzed by introducing one buckled Cu atomic layer positioned between the Cu-O rows in the topmost layer. The interlayer spacing of the buckled layers was initially set at buckling parameter $b=0$, and we allowed buckling of the second and third substrate layers as in the missing-row models. The key idea is to see whether the correlation with the experimental *IV* curves can be improved for lateral relaxation of copper and oxygen atoms in the Cu-O rows due to the change of interlayer spacings and buckling in the deeper copper layers. No problem of convergence was found in running SATLEED programs with the thick ''composite layer'' on the surface. After sufficient optimizations, the

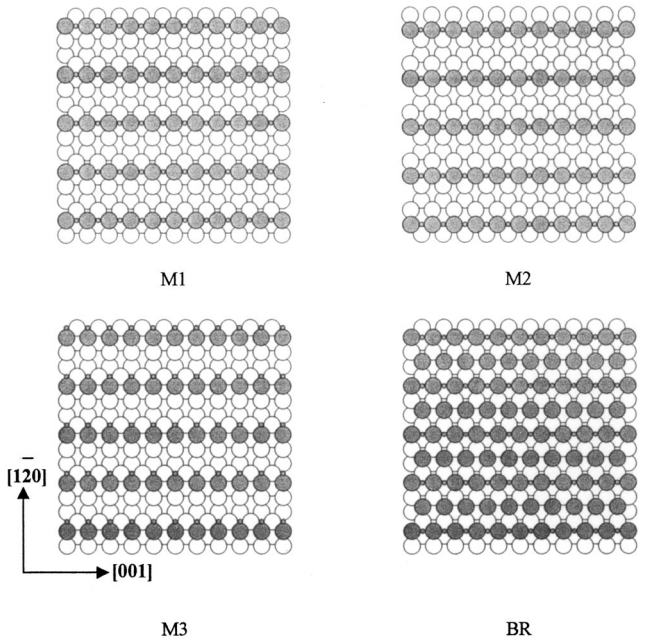

FIG. 2. Top view of the added row ($M1$, $M2$, and $M3$) and the buckled row (BR) models for the Cu(210)-(2×1)O structure. The small gray circles are O atoms, and large-gray circles and large open circles represent the topmost Cu atoms and deeper Cu atoms, respectively.

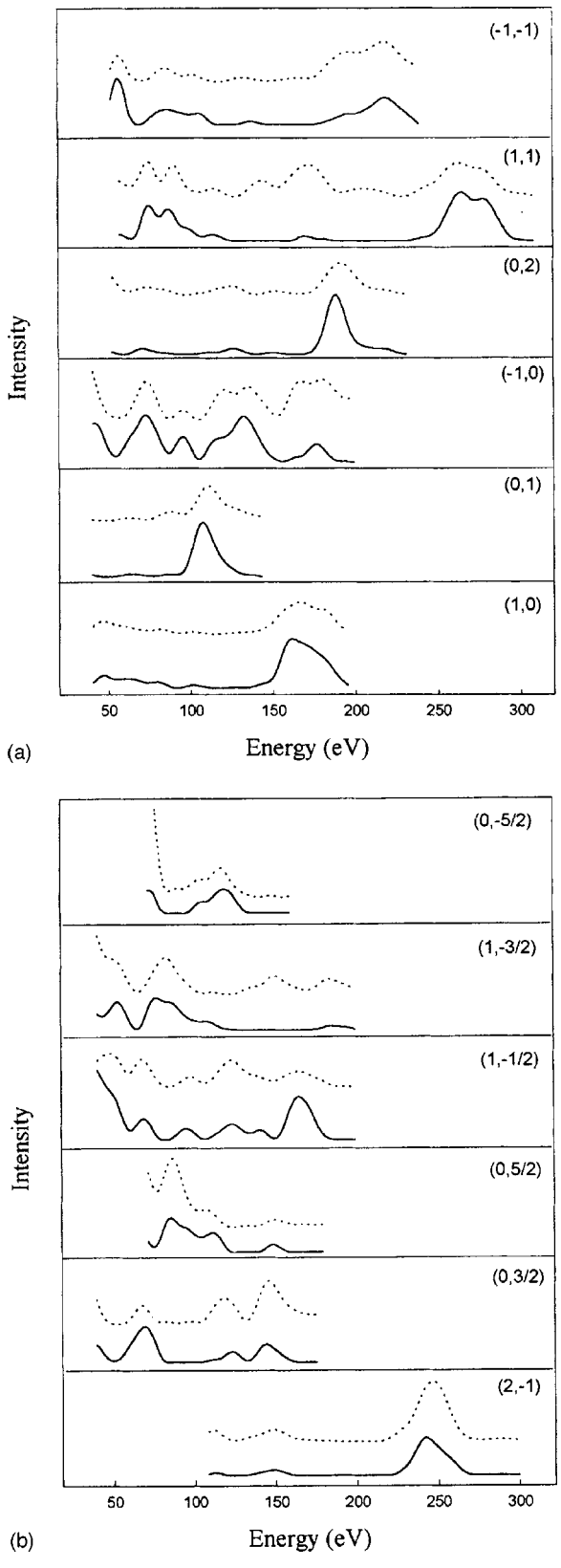

FIG. 3. Experimental (solid lines) and theoretical (dashed lines) best-fit LEED *IV* curves of the Cu(210)-(2×1)O structure determined for the *M*1 model by a tensor LEED calculation.

TABLE I. The parameters of the best-fit geometry after tensor LEED calculations with model *M*1 for Cu(210)-(2×1)O. The bulk value of interlayer spacing of Cu(210) surface is 0.808 Å. the interlayer relaxation and buckling are represented by *d* and *D*, respectively, while the parameter *L* gives the displacement in the $[1\bar{2}0]$ direction.

Vertical relaxation		Lateral relaxation	
Parameter	Optimized value (Å)	Parameter	Optimized value (Å)
d_{01}	-0.07 ± 0.05	L_{01}	0.25 ± 0.03
d_{12}	$1.03\pm0.07(+27.6\%)$	L_{12a}	$1.83\pm0.05(+13.2\%)$
d_{23}	$0.84\pm0.04(+4.1\%)$	L_{12b}	$2.07\pm0.07(-14.4\%)$
d_{34}	$0.79\pm0.05(-2.1\%)$	L_{13a}	$3.46\pm0.06(+7.3\%)$
D_{22}	0.38 ± 0.03	L_{13b}	$0.54\pm0.05(-32.7\%)$
D_{33}	0.16 ± 0.03	ΔL_{22}	-0.14 (-3.5%)
D_{44}	<0.01	ΔL_{33}	-0.04 (-1%)

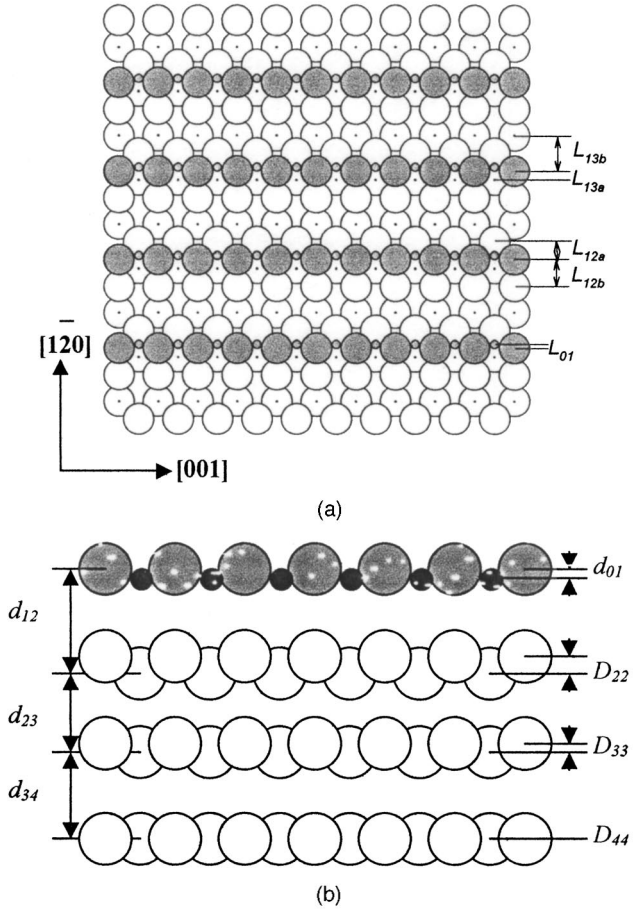

FIG. 4. Schematic of the added row (*M*1) model for the O-induced 2×1 structure viewed from (a) the top and (b) the side according to the best-fit geometry. The parameters are labeled as in Table I. *d* defines interlayer spacing along the direction perpendicular to Cu(210) surface, and *L* defines the lateral relaxation in the $[1\bar{2}0]$ direction. Accordingly, the buckling parameters for the second, third and forth layers are indicated with D_{22}, D_{33}, and D_{44}, respectively.

R_p value was determined to be 0.316 for the BR model. The correlation with the experimental *IV* curves increased as the buckling parameter D_{II} increased in the calculation. Single-beam *R* factors for half-order beams increased much more than those for integer beams. Using the reliability definition for the *R* factors,[21] σ_p^2 $[=4\varepsilon R_{\min}(2V_{oi}/\Delta E)^{1/2}]$ with ΔE of 1900 eV, σ_p^2 for the optimized buckling model was determined to be 0.0205. This value is larger than $\sigma_p^2=0.0139$ obtained for the missing-row model $M1$. In all analyzed models, the best correspondence with experimental *IV* intensities is achieved with model $M1$ with the long bridge added row geometry. The O-induced reconstruction reflects the similarity between the 2×1 Cu-O rows on Cu(210) and those in the Cu(110)-(2×1)O system in that the Cu-O rows aligning parallel to the [001] direction, but with a larger inter-row spacing of 8.08 Å on the Cu(210) surface.

Figure 3 shows a comparison between calculation and measurement results of inequivalent integer beams (10), (01), (-10), (02), (11), $(-1\ -1)$, $(2-1)$, and fractional beams $(0\ \frac{3}{2})$, $(0\ \frac{5}{2})$, $(1\ -\frac{1}{2})$, $(1\ -\frac{3}{2})$, $(0\ -\frac{5}{2})$, based on the tensor LEED calculation of the long bridge added row $(M1)$ model. In the experiment, we measured the intensity spectra of 19 diffracted beams, and after averaging the spectral data of corresponding symmetrically equivalent beams, 12 inequivalent beams were employed in the calculation with a cumulative energy range of 1900 eV. The optimized parameters for this model are listed in Table I with the corresponding labeling of geometrical parameters shown in Fig. 4. From the parameters of the best-fit geometry, we find that oxygen is approximately coplanar with the bridged Cu atoms, with

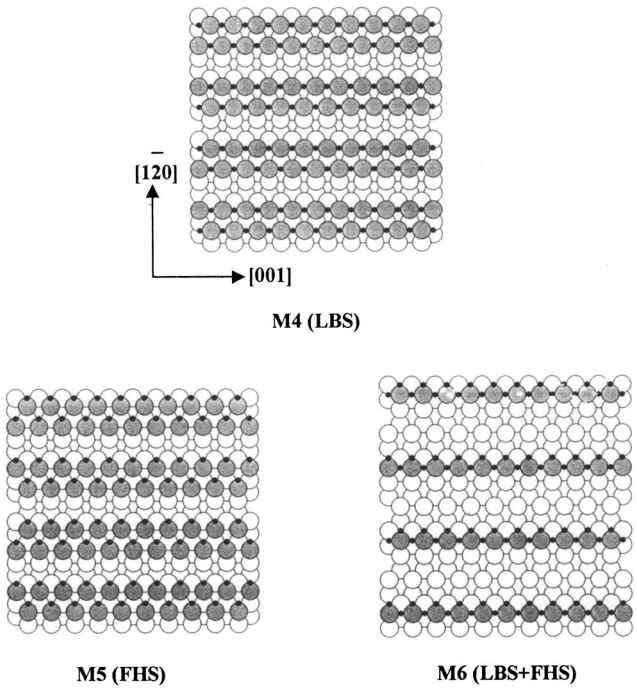

FIG. 5. Top view of the missing row ($M4$, $M5$, and $M6$) models for the Cu(210)-(3×1)O structure with an oxygen coverage of $\frac{2}{3}$ ML. The small black circles are O atoms, and large gray circles and large open circles represent the topmost Cu atoms and deeper Cu atoms, respectively.

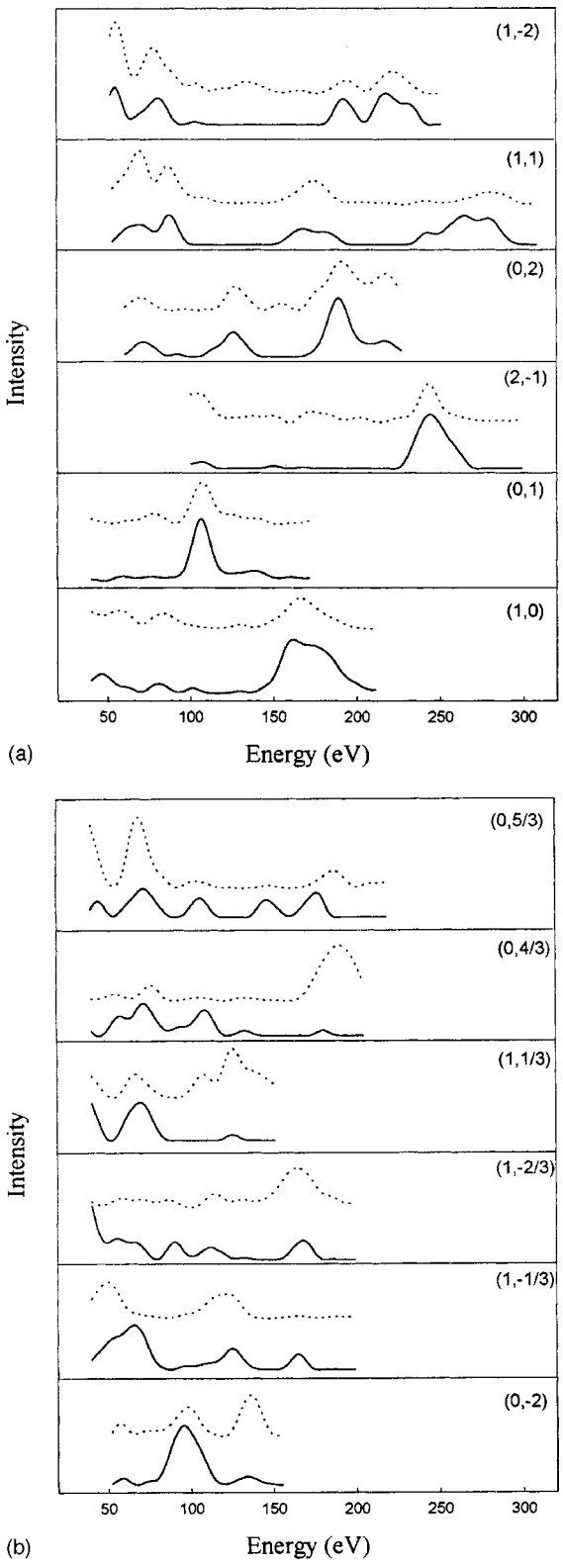

FIG. 6. Experimental (solid lines) and theoretical (dashed lines) best-fit LEED *IV* curves of the Cu(210)-(3×1)O structure determined with the long bridge added row model ($M4$) by tensor LEED calculation.

TABLE II. The parameters of the best-fit geometry after tensor LEED calculations with model $M4$ for Cu(210)-(3×1)O at an oxygen coverage of $\frac{2}{3}$ ML. The interlayer relaxation and buckling are represented by d and D, respectively, while the parameter L gives the displacement in the $[1\bar{2}0]$ direction.

	Vertical relaxation		Lateral relaxation	
	Parameter	Optimized value (Å)	Parameter	Optimized value (Å)
First Cu-O row	d_{01}	-0.12 ± 0.05	L_{01}	$+0.25\pm0.03$
	d_{12}	$0.99\pm0.06(+22.6\%)$	L_{12a}	$1.77\pm0.04(+9.9\%)$
	d_{23}	$0.70\pm0.05(-13.3\%)$	L_{12b}	$2.04\pm0.06(-15.7\%)$
Second Cu-O row	d'_{01}	$+0.17\pm0.07$	L'_{01}	-0.54 ± 0.05
	d'_{12}	$1.03\pm0.07(+27.6\%)$	L'_{12a}	$1.22\pm0.05(-23.9\%)$
	d'_{23}	$0.78\pm0.05(-3.4\%)$	L'_{12b}	$2.80\pm0.07(+15.8\%)$
	D_{22}	0.17 ± 0.04	L_{00}	$4.05\pm0.07(+0.2\%)$

oxygen atoms laterally displaced ($L_{01}=0.25\pm0.03$ Å) relative to the topmost Cu atoms in the $[1\bar{2}0]$ direction. Oxygen locates slightly below the top Cu layer with $d_{01}=-0.07\pm0.05$ Å. The result is similar to that of the Cu(110) surface where oxygen atoms are slightly below the topmost Cu atoms by 0.1 ± 0.1 Å, as determined by STM and low-energy ion scattering.[26,27] The Cu-O chains appear slightly zigzagged due to O-atom bonding to both the topmost Cu atoms and the ''substrate'' Cu atom in the second layer. By checking the optimized coordinates, we do not find a large lateral displacement of Cu and O atoms in the chains from their ''ideal'' sites relative to the substrate layers, which might be expected in the 2×1 reconstruction with a missing row between the two adjacent Cu-O rows. The topmost Cu atoms in the Cu-O chains only shift from their ideal fcc stacking positions by -0.18 ± 0.03 Å along the $[1\bar{2}0]$ direction, and O atoms displace laterally in the opposite direction by 0.06 ± 0.03 Å. On the other hand, the formation of Cu-O rows in the topmost layer brings about buckling in the second and third underlying Cu layers while the positions of Cu atoms on the fourth layer remain almost unchanged. The extent of interlayer buckling is determined to be 0.38 ± 0.03 Å (D_{22}) and 0.16 ± 0.03 Å (D_{33}) for the second and third layers, respectively. Both values are larger than the vertical displacement parameter ($d_{01}=-0.07\pm0.05$ Å) in the first layer. The Cu atoms in the second and third layers just beneath the O atoms at bridged sites have moved downward relative to O, implying strong interaction between the O and Cu atoms at both the second and third layers. Furthermore, O adsorption on the topmost layer leads to a lateral movement of the second and third Cu layers toward the Cu-O row to facilitate the optimum Cu-O bond length. The expansions of the first and second interlayer spacing (d_{12} and d_{23}) are determined by quantitative LEED analysis to be $+27.6\%$ and $+4.1\%$ respectively from the bulk value while the third interlayer spacing (d_{34}) contracts (-2.1%). This is rather different from the multilayer relaxations on clean Cu(210) where the first two interlayer spacings contract (-5.7% and -6.0%, respectively) and the third spacing expands ($+6.8\%$) [see Fig. 4(c)].[28] Similar expansions have been reported for the O-induced 2×1 and $c(6\times2)$ reconstructions on Cu(110).[29,30] The expansion on Cu(210) ($+27.6\%$) is larger than that of $+16.3\%$ for Cu(110)-(2×1)-O, but smaller than the $+31.9\%$ expansion in Cu(110)-$c(6\times2)$-O. O bonding plays an important role in the reconstructions on Cu surfaces and relaxations occur to optimize bond lengths between O and Cu atoms.

For the Cu(210)-(3×1)O reconstruction, over ten trial 3×1 structures at $\frac{1}{3}$-ML and $\frac{2}{3}$-ML coverages were tested using the SATLEED program. It was found that the $\frac{2}{3}$-ML structures gave better fit to experimental data, and the $\frac{1}{3}$-ML structures are not discussed henceforth. Figure 5 shows three models employed in the tensor LEED calculations for the

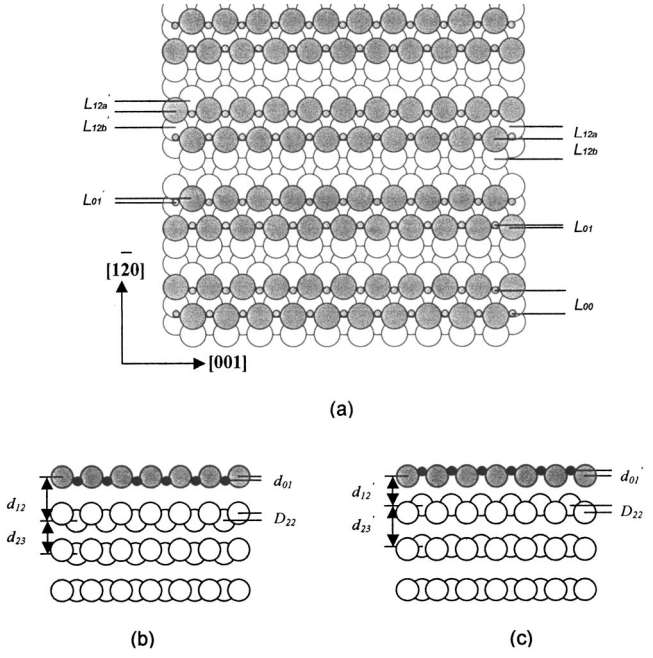

FIG. 7. Schematic of the long bridge added row ($M4$) model for O-induced 3×1 structure as viewed from (a) the top, and the side for both the first Cu-O row (b) and the second Cu-O row (c), according to the best-fit geometry. The parameters are labeled as in Table II. d defines interlayer spacing along the direction perpendicular to Cu(210) surface and L defines the lateral relaxation in the $[1\bar{2}0]$ direction. The buckling parameter for the second layer is indicated with D_{22}.

Cu(210)-(3×1)O reconstruction with an oxygen coverage of $\frac{2}{3}$ ML. As with model $M1$ for the (2×1)O structure, model $M4$ has O atoms approximately coplanar with Cu atoms in each Cu-O row, with the inter-row separation of the paired Cu-O rows initially preset at 4.04 Å. In model $M5$, oxygen atoms occupy the fourfold hollow site instead. In model $M6$, half of the oxygen atoms reside at the long bridge site while the other half occupying the fourfold hollow site. Accordingly, the inter-row separation in model $M6$ is 12.12 Å. After optimization in the tensor LEED calculations, R_p values of 0.361, 0.446, and 0.459 were obtained for models $M4$, $M5$, and $M6$, respectively. Since the unit cell in the (3×1)-O structure is relatively larger, R_p values obtained were generally higher than for the (2×1)-O reconstruction. Nevertheless, the long bridge added row model $M4$ is clearly the best-fit structure for the Cu(210)-(3×1)O reconstruction at $\frac{2}{3}$-ML oxygen coverage. Figure 6 compares calculated and measured IV spectra of inequivalent integer beams (10), (01), (02), (0 −2), (11), (1 −2), (2−1), and fractional beams (1 $\frac{1}{3}$), (1 $-\frac{1}{3}$), (1 $-\frac{2}{3}$), (0 $\frac{4}{3}$), (0 $\frac{5}{3}$), for the best-fit structure described in model $M4$. These 12 inequivalent beams are extracted from 19 measured diffracted beams as previously described after averaging the spectral data of corresponding symmetrically equivalent beams. The 12 inequivalent beams were employed in the calculation with a cumulative energy range of 1980 eV. The optimized parameters for this model are listed in Table II with the corresponding labeling of geometrical parameters shown in Fig. 7. For easy reference, we designate the lower of the paired Cu-O rows in the $[1\bar{2}0]$ direction as the first Cu-O row and the upper as the second Cu-O row. As illustrated in Table II and Fig. 7, we find substantial displacements in the adjacent Cu-O rows. The oxygen atoms are essentially coplanar with the topmost Cu atoms in both Cu-O rows, as in the Cu(210)-(2×1)O structure. O atoms in the first Cu-O row are laterally displaced by $+0.25\pm0.03$ Å in the $[1\bar{2}0]$ direction relative to its nearest topmost Cu atoms. In the second Cu-O row, the lateral displacement of oxygen atoms occurs in the opposite direction $(-0.54\pm0.05$ Å). The lateral separation between O atoms in adjacent Cu-O rows is 4.05 ± 0.07 Å and the separation between the corresponding topmost Cu atoms is 4.84 ± 0.07 Å, 19.8% larger than the corresponding bulk value. This indicates strong repulsive interaction between the paired Cu-O rows. Normal to the surface, the first Cu-O row resides higher than the second row by 0.13 Å. The oxygen atoms in the first row are seated deeper than the topmost Cu layer $(d_{01}=-0.12\pm0.05$ Å), while the oxygen atoms in the second Cu-O row reside $+0.17\pm0.07$ Å higher than the corresponding Cu atoms (d'_{01}). As observed in the (2×1)-O structure, the paired Cu-O rows in the (3×1)-O structure also lead to a buckling of Cu atoms on the second and third layers. The corresponding Cu atoms in the second and third layers are lifted up or pushed down, depending on the locations of the O atoms in the Cu-O rows. The first Cu interlayer spacings (d_{12} and d'_{12}) increase to about 0.99 ± 0.06 and 1.03 ± 0.07 Å, respectively, giving expansions of +22.6% and +27.6% from the bulk value. These expansions are comparable to that in the (2×1)-O structure, which means that the O atoms maintain a similar bonding environment and coordination in the (3×1)-O structure.

On the formation mechanism of Cu-O rows on Cu(210), it is clear from the tensor LEED calculations that oxygen adsorption leads to an expansion of the contracted interlayer spacings of the clean surface. The expanded distance of the Cu-O row from the second and third layers allows the higher mobility of the Cu-O rows. The added row model can explain the formation mechanism of the Cu(210) (2×1)-O, and (3×1)-O reconstructions, where the growth of Cu-O rows results from the diffusion of Cu adatoms from the terrace edges to active O sites and bonding with these adatoms. The second and third Cu layers are buckled due to strong interaction between O and Cu atoms. The resulting nearest-and second-nearest-neighbor Cu-O distances for the fourfold Cu-O bonds are determined to be 1.82 ± 0.03 and 1.96 ± 0.06 Å, respectively, for both 2×1 and 3×1 reconstructions. These values are in good agreement with those obtained from previous SEXAFS studies,[7,25] and those of bulk Cu_2O (1.84 Å) and CuO (1.95 Å).[31,32]

CONCLUSIONS

This LEED study shows that O adsorption can lead to a series of $(n\times1)$ $(n=2,3)$ reconstructions on Cu(210) comprising Cu-O chains along the [001] direction during oxygen uptake at 300–700 K. From the temperature-dependent phase transformations, the Cu(210)-(2×1)O structure is the most favorable reconstruction. By comparing different 2×1 and 3×1 models using tensor LEED analysis, the structure deduced is the added row model with oxygen at the long bridge sites along the [001] direction. The oxygen atoms sit slightly deeper than the topmost Cu atoms, and the top three Cu layers relax vertically. For the Cu(210)-(3×1)O structure with an oxygen coverage of $\frac{2}{3}$ ML, oxygen atoms reside deeper than the accompanying Cu atoms in one Cu-O row, while, in its adjacent row, oxygen sits higher. The nearest- and second-nearest-neighbor Cu-O distances are determined to be 1.82 ± 0.03, and 1.96 ± 0.06 Å, respectively. The Cu-O row formation is found to bring about buckling within the second and third Cu sublayers. By comparison with multilayer relaxation on clean Cu(210), tensor LEED shows that incorporation of the Cu-O bonds dominates the behavior of multilayer relaxation in the first three layers, from contraction for the case of clean surface to expansion for the Cu(210) (2×1)O and (3×1)O systems. The buckling and interlayer expansion in the second and third layers is due to strong interactions between O and Cu atoms in these layers to maintain the optimum Cu-O bond length with fourfold coordination between Cu and O.

ACKNOWLEDGMENTS

The authors are grateful to M.A. Van Hove for helpful discussions and for the use of the Barbieri/Van Hove symmetrized automatrized tensor LEED program and the phase shift source code.

*Corresponding author. Electronic address: phyweets@nus.edu.sg

[1] V. Repain, J. M. Berroir, S. Rousset, and J. Lecoeur, Surf. Sci. Lett. **447**, L152 (2000).
[2] D. J. Coulman, J. Wintterlin, R. J. Behm, and G. Ertl, Phys. Rev. Lett. **64**, 1761 (1990).
[3] M. Bader, A. Puschmann, C. Ocal, and J. Haase, Phys. Rev. Lett. **57**, 3273 (1986).
[4] G. Kleinle, J. Wintterlin, G. Ertl, R. J. Behm, F. Jona, and W. Moritz, Surf. Sci. **225**, 171 (1990).
[5] M. Taniguchi, K. Tanaka, T. Hashizume, and T. Sakurai, Surf. Sci. **262**, L123 (1992).
[6] D. Mocuta, J. Ahner, J. G. Lee, S. Denve, and J. T. Yates, Jr., Surf. Sci. **436**, 72 (1999).
[7] M. Polcik, J. Haase, M. Ondrejcek, and J. H. Petersen, Surf. Sci. **412/413**, 580 (1998).
[8] H. Over, Prog. Surf. Sci. **58**, 249 (1998); F. Besenbacher, F. Jensen, E. Lægsgaard, K. Mortensen, and I. Stensgaard, J. Vac. Sci. Technol. B **9**, 874 (1991); F. Besenbacher and J. K. Nørskov, Prog. Surf. Sci. **44**, 5 (1993).
[9] G. Ertl, Surf. Sci. **6**, 208 (1967).
[10] H. Over, M. Gierer, H. Bludau, G. Ertl, and S. Y. Tong, Surf. Sci. **314**, 243 (1994).
[11] L. Eierdal, F. Besenbacher, E. Lægsgaard, and I. Stensgaard, Ultramicroscopy **42–44**, 505 (1992).
[12] T. Schimizu and M. Tsukada, Surf. Sci. **295**, L1017 (1993).
[13] K. W. Jacobsen and J. K. Nørskov, Phys. Rev. Lett. **65**, 1788 (1990).
[14] R. Feidenhansl, F. Grey, M. Nielsen, F. Besenbacher, F. Jensen, E. Lægsgaard, I. Stensgaard, K. W. Jacobsen, and J. K. Nørskov, Phys. Rev. Lett. **65**, 2027 (1990).
[15] A. T. S. Wee, J. S. Foord, R. G. Egdell, and J. B. Pethica, Phys. Rev. B **58**, R7548 (1998).
[16] P. J. Knight, S. M. Driver, and D. P. Woodruff, Surf. Sci. **376**, 374 (1997).
[17] P. J. Knight, S. M. Driver, and D. P. Woodruff, J. Phys.: Condens. Matter **9**, 21 (1997).
[18] G. W. Lloyd and D. P. Woodruff, Surf. Sci. **285**, L503 (1993).
[19] B. Narloch and D. Menzel, Surf. Sci. **412/413**, 562 (1995).
[20] M. A. Van Hove, W. Moritz, H. Over, P. J. Rous, A. Wander, A. Barbieri, N. Materer, U. Starke, and G. A. Somorjai, Surf. Sci. Rep. **19**, 191 (1993); A. Barbieri and M. A. Van Hove, Symmetrized Automated Tensor LEED package.
[21] J. B. Pendry, *Low Energy Electron Diffraction* (Academic, New York, 1974), p. 25; J. Phys. C **13**, 937 (1980).
[22] S. Y. Liem, G. Kresse, and J. H. R. Clarke, Surf. Sci. **415**, 194 (1998).
[23] G. R. Gruzalski, D. M. Zehner, J. F. Wendelke, and R. S. Hathcock, Surf. Sci. **151**, 430 (1985).
[24] K. C. Tan, Y. P. Guo, A. T. S. Wee, and C. H. A. Huan, Surf. Rev. Lett. **6**, 859 (1999).
[25] S. R. Parkin, H. C. Zeng, M. Y. Zhou, and K. A. R. Mitchell, Phys. Rev. B **41**, 5432 (1990).
[26] F. M. Chua, Y. Kuk, and P. J. Silverman, Phys. Rev. Lett. **63**, 386 (1989).
[27] E. Van der Riet, J. B. J. Smeets, J. M. Fluit, and A. Niehaus, Surf. Sci. **214**, 111 (1989).
[28] Y. P. Guo, K. C. Tan, A. T. S. Wee, and C. H. A. Huan, Surf. Rev. Lett. **6**, 819 (1999).
[29] M. Gierer, H. Over, G. Ertl, H. Wohlgemuth, E. Schwarz, and K. Christmann, Surf. Sci. **297**, L73 (1993).
[30] W. Liu, K. C. Wong, and K. A. R. Mitchell, Surf. Sci. **339**, 151 (1995).
[31] N. Datta and J. W. Jeffery, Acta Crystallogr., Sect. B: Struct. Crystallogr. Cryst. Chem. **34**, 22 (1978).
[32] M. Bader, A. Puschmann, C. Ocal, and J. Haase, Phys. Rev. Lett. **57**, 3273 (1986).